MAVIS: preliminary design of the adaptive optics module

Valentina Viotto, Enrico Pinna, Guido Agapito, Matteo Aliverti, Carmelo Arcidiacono, Andrea Balestra, Andrea Baruffolo, Olivier Beltramo-Martin, Maria Bergomi, Marco Bonaglia, et al.

MAVIS: preliminary design of the adaptive optics module

Valentina Viotto*[ab], Enrico Pinna[bc], Guido Agapito[bc], Matteo Aliverti[d], Carmelo Arcidiacono[ab], Andrea Balestra[a], Andrea Baruffolo[a], Olivier Beltramo-Martin[e], Maria Bergomi[ab], Marco Bonaglia[bc], Runa Briguglio[bc], Giulio Capasso[h], Luca Carbonaro[bc], Elena Carolo[ab], Simonetta Chinellato[abf], Mirko Colapietro[h], Elia Costa[a], Jesse Cranney[g], Ciro del Vecchio[bc], Simone Doniselli[d], Sergio D'Orsi[h], Daniela Fantinel[a], Jacopo Farinato[ab], Thierry Fusco[e], Antony Galla[g], Gaston Gausachs[g], Paolo Grani[bc], Damien Gratadour[g], Davide Greggio[ab], Pierre Haguenauer[h], Nick Herrald[g], Demetrio Magrin[ab], Luca Marafatto[ab], Benoit Neichel[e], Cedric Plantet[bc], Alfio Puglisi[bc], Kalyan Radhakrishnan[ab], Fabio Rossi[bc], Bernardo Salasnich[a], Salvatore Savarese[h], Pietro Schipani[h], Chiara Selmi[bc], Rosanna Sordo[a], Stefan Ströbele[i], Brian Taylor[g], Annino Vaccarella[g], Daniele Vassallo[ab], Simone Esposito[bc], Roberto Ragazzoni[abl], David Brodrick[g], Jennifer Burgess[g], François Rigaut[g]

[a]INAF – Osservatorio Astronomico di Padova, Vicolo dell'Osservatorio 5, 35122, Padova, Italy
[b]ADONI – ADaptive Optics National laboratory in Italy
[c]INAF – Osservatorio Astrofisico di Arcetri, Largo Enrico Fermi 5, 50125, Firenze, Italy
[d] INAF - Osservatorio Astronomico di Brera, Via E. Bianchi 46, 23807 Merate, Italy
[e]Laboratoire d'Astrophysique de Marseille, 38 Rue Frédéric Joliot Curie, 13013 Marseille, France
[f] INAF - Direzione Scientifica, Viale del Parco Mellini 84, 00136 Roma, Italy
[g]Astralis-AITC - Stromlo, RSAA, Australian National University, Cotter Road, Weston, ACT2600, Australia
[h] INAF - Osservatorio Astrofisico di Capodimonte, Salita Moieriello, 16, Napoli, IT 80131
[i]European Southern Observatory, Karl-Schwarzschild Str. 2, 85748 Garching b. München, Germany
[l]Department of Physics and Astronomy, University of Padova, Padova, Italy

ABSTRACT

MAVIS will be part of the next generation of VLT instrumentation and it will include a visible imager and a spectrograph, both fed by a common Adaptive Optics Module. The AOM consists in a MCAO system, whose challenge is to provide a 30" AO-corrected FoV in the visible domain, with good performance in a 50% sky coverage at the Galactic Pole. To reach the required performance, the current AOM scheme includes the use of up to 11 reference sources at the same time (8 LGSs + 3 NGSs) to drive more than 5000 actuators, divided into 3 deformable mirrors (one of them being UT4 secondary mirror). The system also includes some auxiliary loops, that are meant to compensate for internal instabilities (including WFSs focus signal, LGS tip-tilt signal and pupil position) so to push the stability of the main AO loop and the overall performance. Here we present the Preliminary Design of the AOM, which evolved, since the previous phase, as the result of further trade-offs and optimizations. We also introduce the main calibration strategy for the loops and sub-systems, including NCPA calibration approach. Finally, we present a summary of the main results of the performance and stability analyses performed for the current design phase, in order to show compliance to the performance requirements.

Keywords: Adaptive Optics, Multi-conjugate Adaptive Optics, Visible, wavefront sensing

*valentina.viotto@inaf.it

1. INTRODUCTION

The MCAO Assisted Visible Imager and Spectrograph (MAVIS)[1] is part of the next generation of Very Large Telescope instrumentation, and will be installed at the UT4 Nasmyth A platform, to work in combination with the adaptive optics facility (AOF). The consortium is led by the ASTRALIS (Australia, formerly the AAO Consortium), and

includes the Italian national institute for astrophysics (INAF), the Marseille astrophysics laboratory (LAM), in France, and the European Southern Observatory (ESO). With its unprecedented combination of sensitivity and angular resolution in the visible regime, coupled with its spectroscopic features, MAVIS is presented as a general purpose facility instrument[2], which will nicely complement with next generation ELTs near-infrared instrumentation. The system includes four main opto-mechanical sub-systems. The Adaptive Optics Module (AOM) provides multi-conjugate adaptive optics (MCAO) correction in a 30" field of view (FoV) to the Imager and the Spectrograph sub-systems[3]. The former re-images a 30"x30" FoV, with a 7mas/pixel scale, in a number of broad and narrow band filters, while the latter provides integral field unit (IFU) spectroscopic capabilities, in which the FOV size, the spectral resolution (4000<R<12000) and the waveband range (370-100nm) combine differently in four spectroscopic modes. Finally, the Calibration Unit[4] provides suitable sources and references for the internal calibration and characterization of the AOM, Imager and Spectrograph sub-systems. The concept behind the AOM evolved, from its initial idea[5] to the current baseline, which will be presented for the preliminary design review (PDR) in October this year (2022).

In this paper, we present the Preliminary Design of the AOM. We also introduce the main calibration strategy for the loops and sub-systems, including non-common path aberrations (NCPA) calibration approach. Finally, we present a summary of the main results of the performance and stability analyses performed for the current design phase, in order to show compliance to the performance requirements.

2. MAIN AO PARAMETERS

The main performance requirements the AOM MCAO loop shall comply have been already presented in [6], and can be summarized as a bright end Strehl ratio (SR) of 10%, in V band, a full width half maximum (FWHM) of <26mas in faint end (the latter was rephrased in Phase B technical requirements specifications), a SR uniformity better than 10% over the FoV and a sky coverage >50% at the Galactic Pole. To match these specifications, the AOM baseline foresees the use of natural (NGS) and laser guide stars (LGS) combined asterism, including 8 LGSs[7] in a 17.5" radius circular asterism, and up to 3 NGSs, to be acquired in an unobstructed 2' circular FoV and to be sensed in the J+H bands. Two post-focal deformable mirrors (DM) will close the MCAO loop together with the AOF deformable secondary mirror (DSM), resulting in a suite of about 5000 actuators. The complete list of parameters and simulations sensitivity analyses, performed to optimize the system during Phase A, is reported in [8], while the current design performance evaluation is presented in [9].

3. AOM DESIGN CONCEPT

The AOM optical design (shown in Figure 1) was presented in [10] and the expected optical performance are analyzed in [11]. The design was conceived to minimize the number of optical elements, so to push the system throughput, and to optimize the overall stability. The latter is obtained keeping a compact design, with a minimal number of de-rotators, and with a gravity invariant configuration for each of the AOM modules, described in the following (see also [12]). In fact, the only assembly for which the local gravity vector direction changes during operations is a K-mirror.

Following a modular approach, the AOM opto-mechanical design can be divided into three opto-mechanical modules, whose functionalities are listed in the following:

- **Post Focal Relays module (PFR):** the main tasks of the PFR include to re-image the meta-pupils onto the two internal DMs (ALPAO 3228, high stability, see also [13]), to feed the scientific instrumentation (imager or spectrograph, alternatively) and the wavefront sensors with the proper FoV and wavelength band. The LGS channel also includes a focusing system, to compensate for the sodium layer projected distance variation, due to telescope changes in elevation. A K-mirror assembly provides field de-rotation for the instruments and NGS WFS, while a broadband atmospheric dispersion correction (ADC, see also [14]) minimizes the impact of the atmospheric dispersion onto the scientific and technical FoVs. The PFR also includes means for differential focusing of NGS WFS and Science channels, and provides, for the on-axis beam only, pupil imaging and wavefront sensing capabilities.

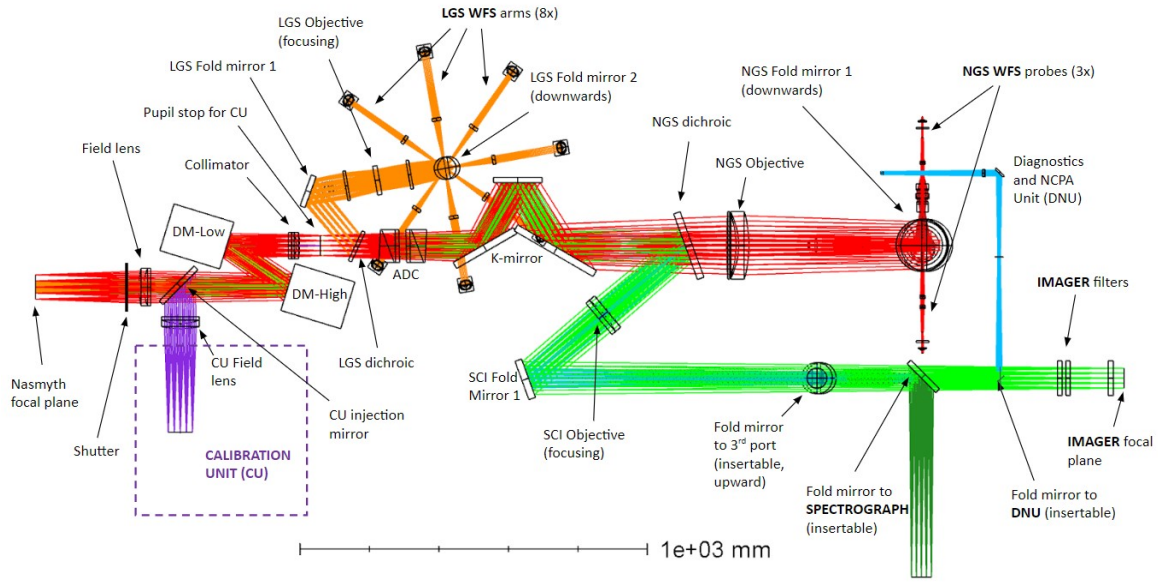

Figure 1. AOM optical layout.

- **Natural Guide Star wavefront sensor module (NGS WFS):** it is the low-order wavefront sensor of MAVIS. Its main tasks include to provide means for natural guide stars' acquisition, with no limitations due to central obstructions or only partial superposition of the probes ranges in the FoV, and to sense the tip-tilt and defocus signal from the selected NGS in the FoV. The NGS WFS also include an acquisition camera, to ease the probes centering while acquiring the sources. Figure 2 shows the opto-mechanical layout of the NGS WFS, highlighting its internal actuators, for each probe, consisting in a X-Y full FoV patrolling stage, a focusing device, to compensate for PFR exit FoV curvature and a micro-lens array (MLA) switch that allows to select between 1x1 and 2x2 sampling options, depending on the available stars brightness. The NIR cameras implemented in the NGS WFS design are based on the Saphira detector array. A more detailed description of the NGS WFS can be found in [15].

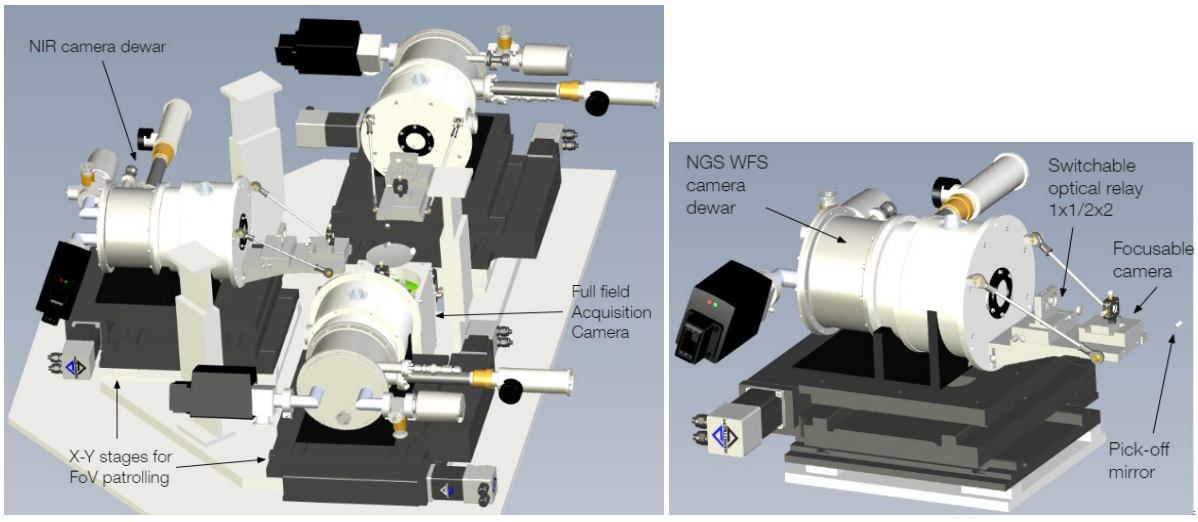

Figure 2. *Left:* NGS WFS opto-mechanical layout; r*ight:* Single Probe view, including configuration and tracking actuators.

- **Laser Guide Star wavefront sensor module (LGS WFS)**: it is the high-order wavefront sensor of MAVIS. The LGS WFS includes means to compensate for apparent field and pupil rotation (changing with UT4 elevation axis), through a mechanical carousel, de-rotating the full module. It also provides means to internally compensate for LGSs differential displacements (in the Na layer plane). This is achieved with eight independent jitter mirrors (one for each LGS arm), which can be driven at high speed by the real-time computer (RTC), using the LGS WFS tip-tilt signal, which is not injected in the MCAO loop. The WFS detectors implemented in the LGS WFS design are the ALICE cameras, developed by ESO. MAVIS is the first multi-conjugate system to exploit super-resolution by design thanks to the ability to introduce differential rotations between pupil and LGS WFS sub-aperture grid.

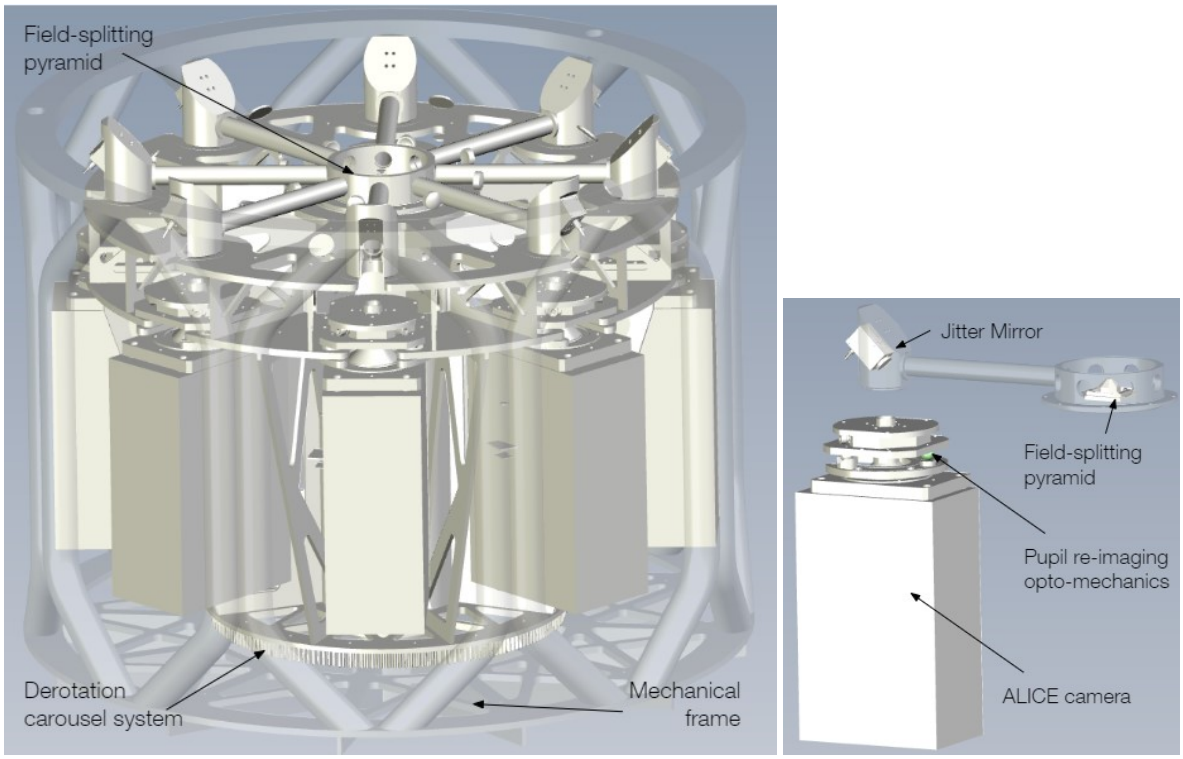

Figure 3. *Left:* LGS WFS opto-mechanical layout; r*ight:* Single arm view.

Because of the system complexity, on top of the MCAO control actuators, the AOM includes a number of moving devices, which are controlled by the instrument control system software (ICSS, see also [16]):

- configuration devices: the AOM provides different modes and configurations, which require means to switch between them, to select the needed setup (e.g. switch between output ports or change NGS WFS pupil sampling)
- tracking devices: as previously mentioned the AOM shall take care of fields de-rotation, LGS distance compensation and atmospheric dispersion compensation
- PFR performance compensators: focusing mechanisms to optimize detectors focusing in the science and NGS channels
- stabilizers: the AOM is a complex sub-system, whose tight requirements in terms of WFE budget translate into the need of a stable yet flexible system, which can adapt to external and internal instabilities, to be compensated with auxiliary stabilization loops, controlled by the ICSS. These loops are described in the next Section.

The electronics design of the AOM shall take into account the controllers for all these actuators, together with the WFSs and technical cameras. The preliminary design overview of the AOM control electronics is presented in [17].

4. AOM CONTROL LOOPS

As already mentioned, MAVIS AOM is an MCAO system, in which the high order wavefront slopes coming from the LGSs asterism and the tip-tilt and plate scale information retrieved in the wide NGS technical FoV are combined by the real time computer to retrieve the optimal shapes of the DMs suite that maximize the AO performance in the science FoV. The baseline design of MAVIS includes the use of 3 different control schemes: Minimum Mean-Square Error (MMSE), Predictive Learn and Apply (PLAA, see also [18]and [19]), and Linear Quadratic Gaussian (LQG). Only one control scheme can be used at a time. While a default control scheme will be defined, the use of the other two schemes will be limited in practice. Details of the RTC design and performance are reported in [20], while a scheme of the control pipeline is shown in Figure 4.

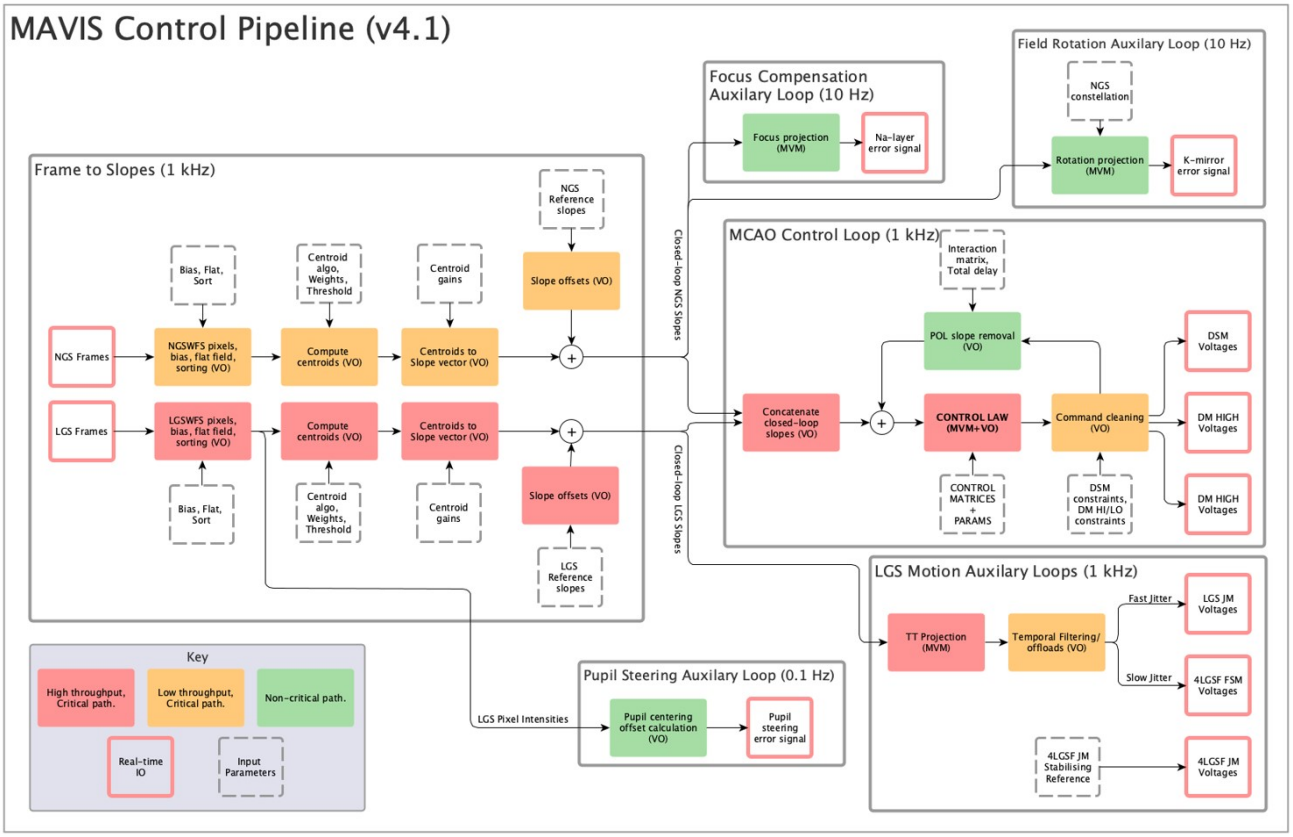

Figure 4. MAVIS AOM control loops scheme.

Because of the tilt indetermination problem[21], the LGSs are not used as references for the tip-tilt in the MCAO loop. While the measurement of the actual position of the LGSs in the WFS focal plane is not an input for the AO loop and their stabilization doesn't correspond to science field aberration correction, we want to keep the LGSs images fixed on the LGS WFS, to avoid their movement propagates as noise or WFE in the system. To keep the jitter below the limit we assume in the error budget, a dedicated compensation loop is introduced. While the choice of the sensor for this LGS jitter compensation loop is straightforward, as the LGS WFS already measures the LGSs positions, more compensators were, in principle, available. However, as, in MAVIS configuration, the AOF needs to be updated to split each laser in two, so to propagate a total of 8 beams to the Na layer, this limits the compensation of LGS jitter with AOF steering and jitter mirrors to couples of LGSs. As the differential jitter between two references produced by the same launcher needs to be compensated too, the AOM shall have a way to do it within the instrument. The RTC is also in charge of driving, at high loop speed, the LGS internal jitter mirrors, so to stabilize the position of the LGSs images onto the detectors.

The tight wavefront error budget of the AOM implies that we push the system performance at its limits, also in terms of calibrations and stability during the observation. For this reason, three additional loops (driven at a lower frequency) have been included in the control scheme. For each of these auxiliary loops, the RTC retrieve the needed measurement

from the WFSs detectors, computes the "error signal" and publishes it, so that the ICSS can read it and drive the respective compensators. The three AOM auxiliary loops are:

- Focus compensation auxiliary loop: the MCAO control scheme assumes to retrieve the information about all the aberration modes, excluding tip-tilt, from the LGS WFSs slopes. However, as the LGSs are generated by the Na layer excitation, the focus term that can be retrieved is affected by the Na layer mean altitude fluctuations with time. The focus induced by sodium layer altitude variations is uncorrelated with the atmospheric turbulence focus. This translates into a drift of the focus term compensated by the system, which needs to be constrained. This is done using NGS WFS measurements, obtained by applying a 2x2 pupil sampling on NGS sources, when the flux allows. To compensate for the measured drift, the ICSS offsets the LGS WFS objective focusing actuator, with respect to its tracking law (which is function of the telescope elevation). This approach also compensates for differential focus terms that may be injected into the system in the LGS-NGS non common path from any system instability (e.g. temperature-dependent aberrations).
- Pupil stabilization auxiliary loop: the performance of the AO loop shows some sensitivity to the pupil image alignment on the LGS WFS MLAs. The results of a dedicated analysis, together with the relevant allocation in the AO budget, allows us to constrain the maximum shift of the pupil position with respect to the MLAs that we can tolerate to about 0.5% of the pupil diameter. On the other hand, there are a number of sources for pupil drift, whose combination is expected to be statistically relevant: the tilt of the nominal optical axis of the telescope with respect to the mechanical axis of the rotator, due to gravitational and thermal flexure as well as alignment errors (this term already exceed our limit), the LGS WFS objective transmitted beam stability, and the LGS WFS carousel axis stability. The AOM, then, implements a pupil image stabilization loop, in which the RTC evaluate the pupil shift computing the change in the differential illumination of the Shack-Hartmann (SH) spots at the edge of the pupil. The compensator for this auxiliary loop is the X-Y position of the field lens, which is adjusted by dedicated actuators, driven by the ICSS.
- Field rotation drift auxiliary loop: in the AOM, the tip-tilt information for the MCAO loop comes from the NGS WFS measurements. At the same time, there is a common term that can be retrieved from the NGS tip-tilt, which is due to a drift of the k-mirror de-rotation motion. If the k-mirror trajectory starts to slightly diverge from the optimal de-rotation, needed to stabilize the science and technical fields, the NGSs images start to move together around the de-rotation axis. This common motion can be computed by the RTC as a slow rate average of the tip-tilt signals, injected into the MCAO loop, and published at a given rate. The ICSS, then, can read these data and, if/when this term exceeds a given threshold, correct the K-mirror trajectory accordingly.

5. CALIBRATION STRATEGIES AND TOOLS

As mentioned above, the AOM is a quite complex sub-system, which needs to satisfy tight wavefront error requirements. For this reason, the calibration and characterization phases, both during alignment and verification, during commissioning, and during operations, are crucial ones, that the team started to plan early in the project development.

5.1 Calibration needs

We can identify some calibrations to be done at modules/assembly level:

- Standard detectors calibrations, to be performed both for WFSs and technical cameras (bias, dark, hot-pixel maps, etc.)
- DMs characterizations as a separated assembly (flat reference shape, actuators response, actuators map, influence function...)
- Actuators calibrations (encoders units vs angles or linear units)

On top of these, the AOM needs a number of characterizations at sub-system level, after the alignment is completed, to feed into the tracking laws and auxiliary loops. The output of these characterizations can be either look-up tables (LUT) or sensitivities/gains:

- DMs characterizations inside the full AOM (meta-pupils location, mis-registration, parameters for synthetic interaction matrices)
- LGS objective tracking law (as a function of LGS source distance, namely telescope elevation)

- Pupil image position sensitivity to field lens movements
- LGS images position sensitivity to LGSs jitter mirrors movements
- NGS focus signal sensitivity to LGS objective movements
- Science image focus signal sensitivity to science channel objective movements
- NGS common tilt signal sensitivity to K-mirror drift
- NGS probes focusing actuator LUT, as a function of probe position in the technical FoV (to compensate for PFR output field curvature)
- ADC look-up-table
- Mapping of the different FoV: acquisition camera into NGS technical FoV and the latter into output science ports (ultimately into imager and spectrograph FoV)

Finally, there are a number of system-level calibrations that need to be performed when the full MAVIS instrument is assembled, and that will be repeated routinely during the lifetime of the instrument, while in operations, to provide offsets to the AO loop and information to be injected into the data reduction pipeline:

- Non-common path aberrations calibration (NCPA)
- Distortion calibration

5.2 Calibration tools

As a number of calibrations/characterizations are needed by the AOM (and also by the Imager and Spectrograph, of course), MAVIS implements a Calibration Unit (CU) sub-system, which takes care of providing a number of functionalities, so to calibrate the system in all its aspects. Among its main functionalities, the ones exploited by the AOM include suitable sources for the LGS WFS calibrations, equipped with focusing and field rotation capabilities to mimic the sodium layer distance evolution and the apparent rotation, NIR sources for the NGS WFS full field characterization, so to calibrate the probes focus compensators that take care of the FoV curvature, and a broad band on-axis source to evaluate the performance on-axis. The CU also includes an additional mask, devoted to astrometric calibrations (see also [22]).

In addition to the CU, two additional calibration/characterization tools are implemented, within the AOM. The Diagnostic and NCPA Unit (DNU) is included in the PFR, and consists of a dual-use opto-mechanical assembly, which picks-up the light from the on-axis science beam (very close to the PFR exit focal plane) and allows to either measure the wavefront shape with a high order Shack-Hartmann WFS (e.g. to measure the residual aberrations after the AOM alignment and/or NCPA calibration), or to re-image the pupil of the system. Nighttime use of the DNU will be mainly during system commissioning, while it is not baselined for nominal operations (although it could be useful also for optimizing the telescope collimation model).

Science and NGS technical footprints on the post-focal DMs are not fully covered by LGS footprints, meaning that there will be an external rim (almost negligible for the science beams, but may be relevant for the NGS WFS beams) of the DMs, used by the system but not monitored by the high order wavefront sensor. On one side, the consortium is working on the most stable and reliable control scheme and selecting the high stability solution for the DMs, so to minimize any drift, but at the same time, we devised a way to monitor the DMs full shape, after they are mounted onto the PFR, installing a portable interferometer on top of the AOM, with means to measure the DMs shape in double pass (Figure 5). This can be achieved only in daytime, to confirm previous calibrations and check the DMs behavior.

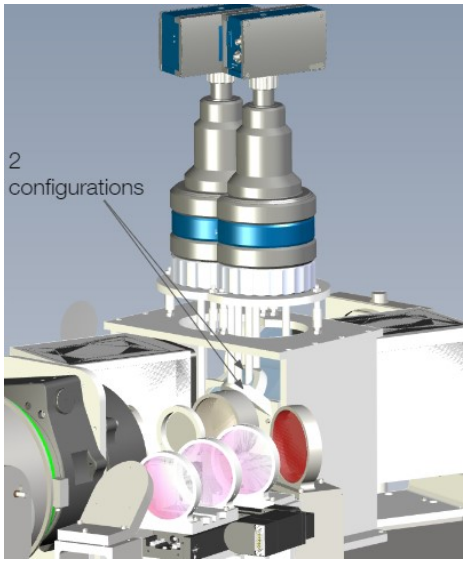

Figure 5. Two configurations to characterize PFR DMs shape in in daytime, with portable interferometer.

5.3 NCPA and calibration strategy and preliminary estimation

The goal of NCPA calibration is to characterize the NCPA and then compensate for them, using the DMs. The plan for NCPA calibration in MAVIS involves the use of the Phase Diversity (PD, [23]), which is a wavefront sensing technique that allows to measure the wavefront by comparing the PSFs of a reference source, when some known aberrations are applied (typically defocus). As this technique can allow to measure the wavefront directly on the imager focal plane, this is particularly suitable for the NCPA characterization. In addition to that, being the AOM a MCAO module, we can consider to measure the aberrations in different directions (positions on the imager detector), in order to optimize for the full field. In this way, the aberration reconstruction becomes a tomographic problem.

The Tomographic Phase Diversity (TPD, [24]) uses the differential information coming from a number of PSFs in the FoV to retrieve not only the incoming aberrations, but also the locations, along the optical path, at which these aberrations are introduced and can be corrected at best. To do that, as we aim at correcting for the full field, we need to use more than a compensating device, i.e. all the 3 DMs we can drive. Ultimately, TPD will allow us to bring the DMs at the best configuration (shapes) to optimize the quality on the imager FoV. In this way, all the aberrations introduced in the science channel, after the LGS dichroic, are minimized. Once this is done, the LGS WFS will measure an aberration, which includes the part of the NCPA compensated by the DMs. Then, what is measured by the LGS WFS is recorded and used as offsets for the high order MCAO loop. As this is a complex system, with a number of possibly evolving NCPA sources, the NCPA we evaluate can be grouped depending whether their evolution depends on the Telescope elevation and/or the Sky de-rotation. For this reason, a 2-entries LUT will be built during NCPA characterization. This operation will come with a residual error, to which we allocated 15nm and that will enter the final budget.

As in the MCAO problem, the final shape of the DMs is the result of an optimization, which identifies the best compromise to achieve an optimal correction everywhere in the FoV, with a limited number of compensators. In the AOM baseline design, the optics in the non-common path are all conjugated at negative distances. This is due to the fact that, in the optical design, all the non-common-path optics are located on the opposite side of the pupil image with respect to the post focal DMs. This choice was driven by the fact that the minimization of the optical elements in the PFR optical path was a pillar of the design. Only a few modes (< 10) can be efficiently corrected (< 5% residual) for conjugation altitudes more than 5 km away from a DM, while aberrations lower than -10 km will be hard to correct. To quantify the amount of NCPA aberration, introduced by PFR optics in the science path, that can be corrected by the DMs, in their baseline position a dedicated simulation was ran, resulting in a reduction of the aberration experienced by the science focal plane of about 50% with respect to input static aberration.

Gauging the result of the simulation with the expected NCPA aberration introduced in the science path, we obtain a residual aberration of 30nm (including some margin), directly acting on the science images and to be included in the error budget.

6. SYSTEM STABILITY AND PERFORMANCE

AOM needs to comply to a tight budget. This translates into a number of analysis and requirements, which need to be identified and quantified early in the project life. We here summarize some of the main system budgets, analyzed during MAVIS Phase B.

6.1 Pupil image

As already mentioned, the stability of the images of the pupil on the high order wavefront sensor micro-lenses array is an important parameter of the system, as it affects the MCAO loop sensitivity to the wavefront aberration. For this reason, within the AOM, a loop is implemented to stabilize the pupil image position onto the LGS WFS, using the field lens as a compensator (see Section 4). Once this auxiliary loop is closed, all the differential displacements between the LGS WFS pupils and the science channel exit pupils are experienced by the latter. For this reason, in the exit pupil stability budget we shall include all the sources of differential pupil displacements in the science and in the LGS WFS channels. Any displacement originated in the common path, instead, shall not be considered as it is compensated.

The AOM items that contribute to the exit pupil motion are summarized in Table 1.

Table 1. AOM pupil image stability budget.

Contributor	What affects the transmitted beam stability	Value [% pup.Ø]
K-mirror	bearing performance (wobble and eccentricity) and the alignment of the bearing rotation axis with the upstream optical path chief ray	0.2
ADC	the prisms bearings wobble and the alignment of the bearing rotation axis with the upstream optical path chief ray	0.0056
SCI objective	linear stage wobble	0.05
LGS WFS objective	linear stage wobble	0.03
LGS derotator	LGS WFS carousel performance in terms of wobble, combined with the alignment residual tilt of the carousel rotation axis with respect to the upstream optical path chief ray	0.4
Flexures	the only assembly in the AOM, for which flexures can be expected, as its orientation with respect to the gravity vector changes, is the K-mirror	0.1
Thermal effects	differential shift of the pupil image in the LGS WFS channel and in the science channel	0.1
	Total:	<0.5 (rss)

6.2 PSF drift

Similarly, the stability of the AOM science FoV is locked to the NGS WFS technical FoV, as the PSF stabilization is obtained minimizing the NGSs images motion in the technical FoV. Once the AOM low order loop is closed, all the differential displacements between the NGS WFS images and the science channel PSFs are experienced by the latter. For this reason, in the PSF slow drift budget we shall include all the sources of differential drift in the science and in the NGS WFS channels. Any displacement originated in the common path, instead, shall not be considered as it is compensated. The AOM items that contribute to the PSF drift motion are summarized in the following.

The possible slow PFS drift, while the loop is closed, is dominated by the ADC differential residual chromatism. The differential optimization of the atmospheric dispersion reached by the ADC in the NGS WFS and in the science wavebands can cause a shift of the two FoVs, which ultimately results in a differential motion of the PSF in the NGS WFS technical FoV with respect to the science FoV, when the AOM optical derotator (which is compensating for both the NGS and the SCI channels) is on.

The impact of this term was evaluated for a worst case scenario, corresponding to a narrow band science observation, with a filter spectrally located on the peak of the discrepancy between the NGS WFS and the visible band residual chromatism. Once the technical FoV position is stabilized by the MCAO loop and the NGS field rotation drift auxiliary loop, this discrepancy causes the PSFs in the science FoV to move in a circular pattern. The length of the arc drawn by the PSF, along the circular trajectory, corresponds to the change in the parallactic angle. The estimation of this term is of course statistical, as it strongly depends on the actual optics manufacturing and its combination with the alignment. For this reason, as there is a statistical chance that this term impacts the overall performance in a non-negligible way, we are considering to characterize it and inject the information in the MCAO loop, so to adapt the reference slope for the tip-tilt accordingly, as a mitigation.

The other two terms that can contribute to the PSF drift budget are flexures and thermal effects. The only assembly in the AOM, for which flexures can be expected, as its orientation with respect to the gravity vector changes, is the K-mirror. This, however, is a common element to the NGS WFS and the science path, so no differential impact can be included. Finally, we considered the sensitivity of the PFR optical design to thermal variation and temperature gradients, and we quantified the differential shift of the PSF images in the NGS WFS channel (where the stabilization loop measurement is taken) and in the SCI channel in 2mas per a 1deg/m gradient.

6.3 Wavefront error budget

Finally, the crucial budget for our MCAO system is of course the residual wavefront error (WFE) budget.

This includes the results of simulations (again, see [9]), assuming consistent AO design parameters, as the main contributors, but also other terms:

- MCAO loop residuals: together with the high and low order MCAO residuals, we here list the impact of the reconstructor update, together with the residual of the vibration rejection algorithm[25].
- Limits of the design concept: we here consider limitations which are related to the system conceptual design, which are the telescope aberrations, outside the influence space of the DMs, and the atmospheric turbulence chromatism. The latter is due to the fact that, while the AO system is minimizing the PSF high order aberration at a wavelength included in the science waveband, the tip-tilt and focus are optimized in the NIR.
- Limits of implementation: we here consider the terms due to the practical limitation of the system components, such as the DMs stability and the optical design residual chromatism (both ADC and science channel). Flexures can also enter this part of the budget.
- Auxiliary loops residual terms: here we consider the impact, on the WFE budget, of the residual of the auxiliary loops, described in Section 4, namely the sodium focus tracking and the pupil stabilization. These residuals are often the result of a trade-off between loop update frequency and signal to noise of the measurement.
- Calibration residuals terms: here we include the NCPA calibration residuals, together with the ADC NIR-VIS mismatch compensation residual (Section 6.2). Also the residuals of the thermal look-up table for the best science channel focus seasonal dependence belongs to this terms.

Table 2 reports the AOM Preliminary residual WFE budget, for Phase B.

Table 2. AOM residual WFE budget.

Contributor	Comment/assumption	Estimation
Atmospheric turbulence chromatism	LGS WFS @589nm, NGS WFS @ 1000-1740nm, Science @ 370-1000nm	25.5 nm
UT4 un-correctable aberrations	this term is an allocation	15nm
HO MCAO residual		107 nm
Residual jitter		30 nm
Vibrations rejection residual		21 nm
Sodium focus tracking		11 nm
NCPA compensation residual - static		35 nm
NCPA compensation residual - dynamic	due to NCPA calibration with angles discretization. Allocation.	10 nm
SCI channel chromatism		10 nm

ADC residual	@V-band @ Z=30deg	15 nm
ADC differential NIR-VIS compensation residual	Compensated by moving NGS WFS slope reference according with K-mirror angle	10 nm
DMs instability		14 nm
Actuators mismatch		5 nm
Reconstructor update	Based on Pupil sub-apertures rotation sensitivity	20 nm
	Total:	127.1 nm

7. CONCLUSION

We presented the Preliminary Design of the MAVIS AOM, which will undergo its PDR before the end of this year. Even if MAVIS AO performance are ambitious, no showstopper has been identified, at this stage. The opto-mechanical layout of the sub-system has been presented, reporting also the functional details of all its modules, namely the PFR, the NGS WFS and the LGS WFS. We also reported on the AOM control scheme, including both real time loops, led by the AOM RTC, and auxiliary loops, driven by the ICS software. The tight requirements for the AOM performance and the need for a complex control scheme, also translate into a number of calibrations and optimizations, which require a set of calibration references (CU) and online (DNU) or offline (interferometer) measurement tools.

Finally, we summarized the main budget of the AOM, namely the exit pupil stability budget, the PSF slow drift budget and the overall residual WFE budget. While the first two budgets are mainly driven by operational needs of the post focal instrumentation, the latter represents the core of the AOM as a system, as it is the result of AO simulations, control optimizations, and opto-mechanical design (including alignment and manufacturing), together with some limitations due to the AO conceptual scheme. At the present stage of development, the system results in being compliant with its most important performance requirements.

REFERENCES

[1] Rigaut, F., McDermid, R., Cresci, G., Agapito, G., Aliverti, M., Antoniucci, S., Balestra, A., Baruffolo, A., Beltramo-Martin, O., Bergomi, M., Bianco, A., Bonaglia, M., Bono, G., Bouret, J. -C., Brodrick, D., Busoni, L., Capasso, G., Carolo, E., Chinellato, S., Colapietro, M., Content, R., Cranney, J., de Silva, G., D'Orsi, S., Ellis, S., Fantinel, D., Fusco, T., Galla, A., Gausachs, G., Gratadour, D., Greggio, D., Gullieuszik, M., Haguenauer, P., Haynes, D., Herrald, N., Horton, A., Kamath, D., Magrini, L., Marasco, A., Marafatto, L., Massari, D., McGregor, H., Mendel, T., Monty, S., Neichel, B., Pinna, E., Plantet, C., Portaluri, E., Robertson, D., Salasnich, B., Savarese, S., Schipani, P., Schwab, C., Smedley, S., Sordo, R., Ströbele, S., Vaccarella, A., Vassallo, D., Viotto, V., Waller, L., Zanutta, A., Zhang, H., Seemann, U., Kuntschner, H., Arsenault, R. "MAVIS on the VLT: A Powerful, Synergistic ELT Complement in the Visible," The Messenger, 185, 7, (2021).

[2] McDermid, R., Cresci, G., Rigaut, F., Bouret, J.-C., De Sinvs, G., Gullieuszik, M., Magrini, L., Mendel, J. T., Antoniucci, S., Bono, G., Kamath, D., Monty, S., Baumgardt, H., Cortese, L., Fisher, D., Mannucci, F., Migliorini, F., Migliorini, A., Sweet, S., Vanzella, E., Zibetti, S., and other contributors, "Phase A Science case for MAVIS – The Multi-conjugate Adaptive Optics Visible Imager-Spectrograph for the VLT Adaptive Optics Facility," in arXiv.org, https://arxiv.org/abs/2009.09242, (2020).

[3] Ellis, S. et al., "MAVIS: imager and spectrograph," in SPIE proceedings, 12184-8, this conference.

[4] Haynes, D. et al., "MAVIS Calibration Unit: Preliminary design," in SPIE proceedings, 12184-210, this conference.

[5] Esposito, S., Agapito, G., Bonaglia, M., Busoni, L., Fusco, T., Neichel, B., Spanò, P., Bono, G., and Vernet, J., "AOF upgrade for VLT UT4: an 8m class HST from ground," in SPIE proceedings, 9909, 99093U, (2016).

[6] Viotto, V. et al., "MAVIS: the Adaptive Optics Module feasibility study," in SPIE proceedings, 11448,0114480D, (2020).

[7] Haguenauer, P. et al., "MAVIS: Two for One, the art of LGS multiplication," in SPIE proceedings, 12185-283, this conference.

[8] Agapito, G. et al., "MAVIS: system modelling and performance prediction," in SPIE proceedings, 11448, 114483R, (2020).

[9] Agapito, G. et al., “MAVIS: performance estimation of the adaptive optics module,” in SPIE proceedings, 12185-130, this conference.
[10] Greggio, D. et al., “MAVIS Adaptive Optics Module optical design,” in SPIE proceedings, 11448, 11448W, (2020).
[11] Greggio, D. et al., “MAVIS Adaptive Optics Module: optical configuration and expected performance,” in SPIE proceedings, 12185-254, this conference.
[12] Aliverti, M. et al., “MAVIS: preliminary mechanical design overview of the adaptive optics module,” in SPIE proceedings, 12184-150, this conference.
[13] Madec, P.-Y. et al, “Deformable Mirror Technology Development at ESO – From open-loop to eXtreme Adaptive Optics,” in SPIE proceedings, 12185-77, this conference.
[14] Greggio, D. et al., “Optical design of a broadband atmospheric dispersion corrector for MAVIS,” in SPIE proceedings, 11447, 1144755, (2020).
[15] Bonaglia, M. et al, “MAVIS: preliminary design overview of the natural guide star wavefront sensor submodule,” in SPIE proceedings, 12185-252, this conference.
[16] Costa, E. et al., “MAVIS: preliminary design overview of the instrument control software,” in SPIE proceedings, 12189-37, this conference.
[17] Colapietro, M. et al., “MAVIS: preliminary design overview of the AOM control electronics,” in SPIE proceedings, 12148-139, this conference.
[18] Cranney, J. et al., “MAVIS Predictive Control in Learn and Apply Framework,” in SPIE proceedings, 11448, 114482L, (2020)
[19] Zhang, H. et al., “MAVIS Learn and Apply application and performance analysis,” in SPIE proceedings, 11448, 114482C, (2020)
[20] Gratadour, D. et al., “MAVIS RTC: a forward looking implementation of the COSMIC platform,” in SPIE proceedings, 12185-28, this conference.
[21] Rigaut. F. and Gendron, E., “Laser guide star in adaptive optics: the tilt determination problem,” A&A, 261, 677, (1992).
[22] Cranney, J. et al., “MAVIS: astrometric calibration technique,” in SPIE proceedings, 12185-235, this conference.
[23] Gonsalves, R. A., “Phase retrieval and diversity in adaptive optics,” Opt. Eng., 21, 829, (1982).
[24] Gratadour, D. and Rigaut, F., “Tomographic phase diversity for phase retrieval on wide-field AO systems,” in AO4ELT2 proceedings, 49, (2011).
[25] Pettazzi, L., et al, “Improving the accuracy of interferometric measurements through adaptive vibration cancellation,” 2015 IEEE Conference on Control Applications, 95-100, (2015).